

Experimental inhibition of decoherence on flying qubits via bang-bang control

Sajeev Damodarakurup, Marco Lucamarini, Giovanni Di Giuseppe, David Vitali, and Paolo Tombesi

*Dipartimento di Fisica, Università di Camerino,
via Madonna delle Carceri, 9, I-62032 Camerino (MC), Italia*

In recent years the interest in the manipulation of quantum systems has furthered new strategies for maintaining their coherence, continuously threatened by unwanted and uncontrollable interactions with the environment [1]. Photons interact weakly with the surroundings. Even so decoherence may significantly affect their polarization state during the propagation within dispersive media because of the unavoidable presence of more than a single frequency in the envelope of the photon pulse. In this Letter we report on a suppression of the polarization decoherence in a ring cavity obtained by properly retooling for the photon qubit the “bang-bang” protection technique [2, 3, 4, 5, 6, 7] already employed for nuclear spins [8, 9] and nuclear-quadrupole qubits [10]. Our results show that bang-bang control can be profitably extended to all quantum information processes involving flying polarization qubits.

The struggle against environmental decoherence has a long history, which proceeds from the refocusing techniques of Nuclear Magnetic Resonance (NMR) spectroscopy [11] to Quantum Error-Correcting Codes (QECC) [12, 13, 14, 15], Decoherence-Free Subspaces (DFS) [16, 17, 18], Quantum Feedback (QF) [19], and dynamical “Bang-Bang” (BB) decoupling [2, 3, 4, 5, 6, 7]. Despite the impressive achievements of these techniques, QECC and DFS require a large amount of extra resources [13], while QF is limited by measurement inefficiencies.

In dynamical BB decoupling, the system undergoes a sequence of suitably tailored unitary operations which do not require any additional resource or any measurement. The control operations can be chosen so that any undesired effect of the environment like dissipation, decoherence or heating can be eliminated in principle. The physical idea behind BB comes from refocusing techniques of NMR spectroscopy [11], where the controls are implemented in time via a sequence of strong and rapid pulses that provide a full decoupling from the environment in the limit of infinitely fast pulses. The decoherence suppression results in the increase of the NMR “transversal” relaxation time T_2 , which is related to dephasing. Besides NMR, dynamical decoupling has been suggested for inhibiting the decay of unstable atomic states [6, 20], suppressing the decoherence of magnetic states [21], reducing the heating in ion traps [22], and contrasting the quantum noise due to scattering processes in optical fibers [23].

In this Letter we apply the BB technique to a flying qubit, specifically the polarization state of a photon circling in a ring cavity. In fact, the properties of optical elements (here the mirror reflectivity) depend both on frequency and polarization and this fact, in conjunction with a finite integration time of the detectors, results in a trace over the frequency degree of freedom and effectively spoils the coherence of a polarization state. A dephasing process equivalent to that occurring in NMR takes place in the cavity, and after few round-trips the polarization state is almost completely mixed. On the contrary, a generic polarization state is preserved for many round-trips when the BB controls, realized by suitably oriented wave-plates, are inserted in the optical path.

The experimental apparatus employed to demonstrate this effect is depicted in Figure 1a. A pulsed laser, with spectrum as in Figure 1b and intensity reduced to about one photon per pulse, is injected in a triangular ring cavity. The polarization state of the laser is prepared by using a Polarizing Beam-Splitter (PBS) and a set of $\lambda/2$ and $\lambda/4$ wave-plates. At every round trip the light is extracted from the cavity using a thin glass plate. Its polarization is analyzed by means of the tomographic technique [24] (see Methods), and then sent into a multimode fibre connected to a single-photon detector. The output signal from the detector stops the time conversion in a Time-to-Amplitude Converter (TAC) synchronized with the laser. The time delay between the input and output signals is then recorded by a Multi-Channel Analyzer (MCA). The typical acquisition run is shown in Figure 1c. It represents a sequence of peaks separated by the time the photon employs to complete a single cavity round-trip.

We denote with $|V\rangle$ ($|H\rangle$) the linear polarization state orthogonal (parallel) to the plane of the cavity, and with $\mathbb{Z} = |H\rangle\langle H| - |V\rangle\langle V|$ the z Pauli matrix. A cavity mirror acts on the polarization state as $\mathbb{U}_{\mathbb{Z}}(\omega) = \mathbb{Z}\mathbb{M}_{\mathbb{Z}}[\phi(\omega)]$, where $\phi(\omega) = \phi_H(\omega) - \phi_V(\omega)$ is the relative phase due to the polarization-reflectivity difference and $\mathbb{M}_{\mathbb{Z}}[\phi(\omega)] = \exp[-i\phi(\omega)\mathbb{Z}/2]$ (see Methods). The two plane mirrors at 45° are characterized by the same $\mathbb{U}_{\mathbb{Z}}(\omega)$, while the third concave mirror of the cavity is almost at normal incidence: for this mirror $\phi(\omega) \simeq 0$ and therefore it acts as $\mathbb{U}_{\mathbb{Z}} \simeq \mathbb{Z}$. In order to compensate for this operation we have inserted a waveplate \mathbb{Z} in front of the spherical mirror. The input optical pulse is described by a Gaussian amplitude spectrum $\mathcal{E}(\omega)$, normalized such that $\int d\mu_\omega \equiv \int d\omega |\mathcal{E}(\omega)|^2 = 1$, and by a factorized, frequency-independent polarization state $|\pi\rangle_{in}$, so that the photon input state can be written as $|\psi\rangle_{in} = \int d\omega \mathcal{E}(\omega) |\omega\rangle \otimes |\pi\rangle_{in}$. The output polarization state after n round-trips is then given by the reduced density

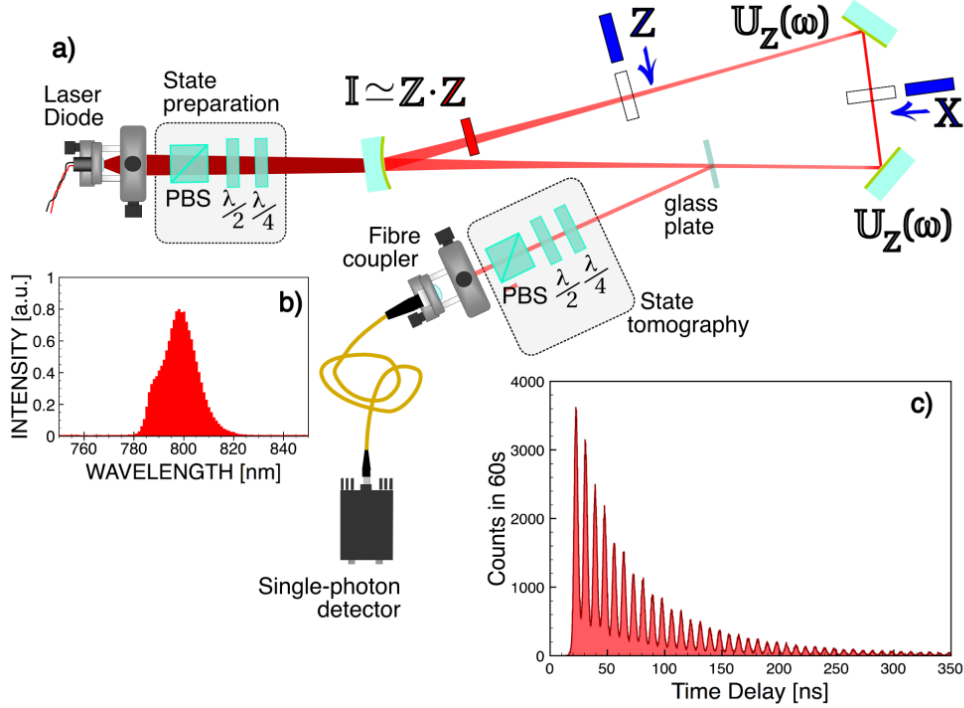


FIG. 1: **a) Schematics of the experimental apparatus.** A laser diode at $\lambda_0 \simeq 800$ nm wavelength and bandwidth $\Delta\lambda \simeq 15$ nm, pulsed at repetition rate of 100 KHz, is injected into the cavity through a spherical mirror with radius of curvature 1 m and reflectivity 98%. The state of polarization of the laser field is prepared through a polarizing beam-splitter (PBS) and a set of $\lambda/2$ and $\lambda/4$ wave-plates. The field confined in the cavity is extracted using a $100 \mu\text{m}$ thin glass plate and sent into a multi-mode fibre connected to a single-photon detector. The polarization state of the output field is reconstructed by means of a state tomography technique [24], implemented with the sequence $\lambda/4$, $\lambda/2$, PBS. Decoherence, labeled with $U_Z(\omega)$ in the Figure, is induced by the two cavity plane mirrors at 45° . The spherical mirror is at nearly normal incidence and it does not induce polarization decoherence. It acts as Z and its operation is compensated by a $\lambda/2$ waveplate in front of it. The BB control operations X and Z are respectively realized by a Soleil-Babinet, which implements a $\lambda/2$ wave-plate, and by a second $\lambda/2$ waveplate in the upper long arm. **b) Spectrum** of the laser diode. **c) Typical acquisition run** given by the electronics. Each peak corresponds to a cavity round-trip. The interval between adjacent peaks amounts to 6.80 ns, and provides an estimate of the cavity-length of about 2 m.

matrix obtained by tracing over the frequency degree of freedom

$$\hat{\rho}_{out} = \int d\mu_\omega U_n[\phi(\omega)] |\pi\rangle_{in} \langle \pi | U_n^\dagger[\phi(\omega)] \doteq \begin{bmatrix} \rho_{11} & \rho_{12} \\ \rho_{12}^* & \rho_{22} \end{bmatrix}, \quad (1)$$

where $U_n[\phi(\omega)] = [U_Z[\phi(\omega)]U_Z[\phi(\omega)]]^n = \exp[-in\phi(\omega)Z]$, and the matrix is written in the $\{|H\rangle, |V\rangle\}$ basis. The frequency average and the dispersive properties of the 45° -mirrors transform the pure input state $|\pi\rangle_{in}$ into a mixed output state $\hat{\rho}_{out}$, with unmodified diagonal matrix elements but with off-diagonal elements decaying to zero for an increasing number of cavity round-trips.

Polarization decoherence is suppressed when BB is applied. The BB is realized by adding two control operations within the cavity: a second Z waveplate before the spherical mirror, and a Soleil-Babinet (S-B) with axis at 45° with respect to the cavity plane and delay equal to $\lambda/2$ in the short arm of the cavity. The S-B acts on the polarization state as the Pauli matrix $X = |H\rangle\langle V| + |V\rangle\langle H|$ and therefore the two controls implement every two cavity round-trips the full Pauli-group decoupling of a qubit [3, 25]. The transformation after the n^{th} -round trip is then changed from $U_n[\phi(\omega)]$ to $U_n^{\text{BB}}[\phi(\omega)] = [ZU_Z[\phi(\omega)]XU_Z[\phi(\omega)]]^n = (iY)^n$; therefore, for even n , the polarization transformation is proportional to the identity operator, thus implying a *perfect preservation of every input polarization state*, i.e., a complete suppression of decoherence. This is illustrated in Figure 2, where are shown the meaningful parts of the experimentally reconstructed output density matrices for diagonal (D) and left circular (L) input states, with and without 11 cycles of BB control. Without BB, the off-diagonal elements are reduced to almost zero after few photon round-trips, while in the presence of BB cycles the qubit state is well preserved, as witnessed by the *freezing* of the density matrices off-diagonal elements to their initial value. A more quantitative description is provided by Figure 3,

where the purity $\text{Tr}(\rho_{\text{out}}^2)$ of the output polarization state is plotted versus the number of BB cycles, for three input polarization states (H , D , R). Polarizations D and R undergo a Gaussian decay (see Methods) to the fully unpolarized state when BB is not performed, while in the presence of BB the purity of these states remains very close to one even after 22 cavity round-trips. On the other side, input state H remain almost unaffected by decoherence both with and without BB. This is a consequence of the fact that the ring cavity of Figure 1 does not realize the most general polarization decoherence, but only a specific one, in which only off-diagonal matrix elements in the known \mathbb{Z} -basis are affected.

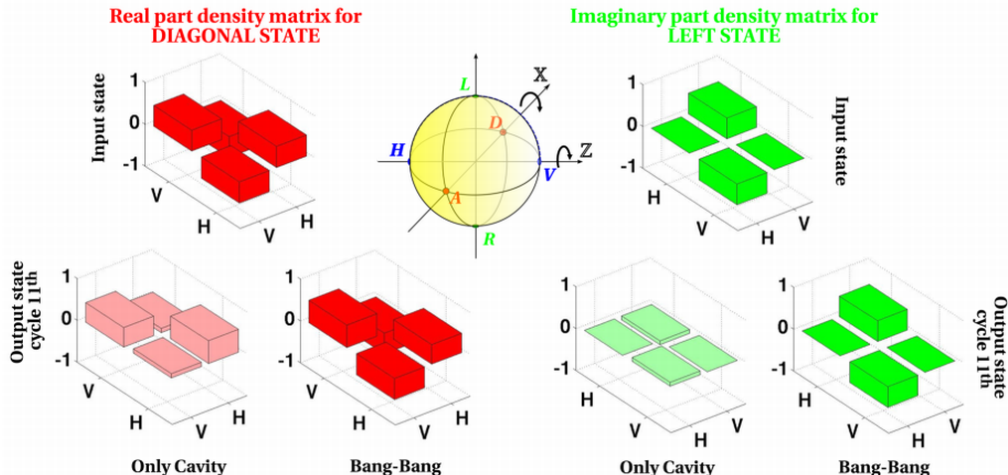


FIG. 2: **Evolution of the density matrices.** Center: Bloch-sphere representing the polarization states of light. The eigenstates of the principal bases \mathbb{X} , \mathbb{Y} and \mathbb{Z} are shown as poles along the main three axes x , y and z . The BB unitary operations, \mathbb{X} and \mathbb{Z} , correspond to π -rotations about the x - and z -axes. Left: real part of the density matrix elements of the input state D (red, on the top), of the output state when BB is not applied (lighter red, on the bottom-left) and of the output state when 11 BB cycles (22 cavity round-trips) are applied (darker red, on the bottom-right). Right: imaginary part of the density matrix elements of the input state L (green, on the top), of the output state when BB is not applied (lighter green, on the bottom-left) and of the output state when 11 BB cycles (22 cavity round-trips) are applied (darker green, on the bottom-right). Notice that the choice of the states D and L aims at showing the generality of the BB decoupling, which succeeds with both linear and circular polarization states. As a consequence even a more general elliptical polarization state can be adequately protected with this technique.

For this reason, we have modified the setup to obtain the most general qubit decoherence, which acts along an arbitrary direction of the Bloch sphere, and affects both diagonal and off-diagonal matrix elements. This allows us to demonstrate the general applicability of the Pauli-group decoupling. The generic single-qubit error model is implemented by placing in front of each plane mirror a S-B with axis at 45° with respect to the cavity plane, thus realizing the unitary operation $\mathbb{B}_{\mathbb{X}}[\theta] = \exp[-i\theta\mathbb{X}/2]$ (see Figure 4). The S-B together with a plane mirror form the decohering element described by the operator $\mathbb{N}(\omega) = \mathbb{M}_{\mathbb{Z}}[\phi(\omega)] \mathbb{B}_{\mathbb{X}}[\theta]$. As a consequence, the transformation of the polarization state after the n^{th} -round trip within the modified ring-cavity is given by $\mathbb{U}_n[\phi(\omega)] = [\mathbb{N}(\omega) \mathbb{N}(\omega)]^n$.

Pauli-group decoupling is again realized every two round-trips by adding the BB operations \mathbb{X} and \mathbb{Z} in the cavity [3, 25]. \mathbb{X} is implemented by adding to the phase of the S-B in the short arm of the cavity a delay equal to $\lambda/2$, while \mathbb{Z} is implemented by an additional $\mathbb{Z} \lambda/2$ waveplate. The overall transformation after the n^{th} -round trip is then given by $\mathbb{U}_n^{\text{BB}}[\phi(\omega)] = [\mathbb{Z} \mathbb{N}(\omega) \mathbb{X} \mathbb{N}(\omega)]^n$.

Figure 5 shows the evolution of the purity of the output state under this general decoherence model, for a generic input elliptical polarization state E , both with (right) and without (left) BB. Each curve corresponds to a different orientation θ of the S-B. BB again inhibits decoherence because, for each orientation of the decoherence-axis, the output purity with BB is significantly higher than the corresponding value without BB. Purity preservation is not as good as in the previous case and worsens for increasing θ . This is so because when decoherence acts along an unknown basis, Pauli-group decouples a qubit from the environment at first order in the variance σ_ϕ^2 of the relative phase difference ϕ . The higher order terms increase with increasing θ thus explaining a poorer performance of Pauli-group decoupling (see Methods). However it should be noted that even higher order decoupling can be achieved using more complex sequences of BB controls [3, 25].

The fact that a generic input polarization state is well preserved by BB Pauli-group decoupling for every orientation of the decoherence axis shows its potential usefulness for improving quantum communications along one-way channels. In fact, a generic communication channel can be divided into many small portions with constant dispersive properties.

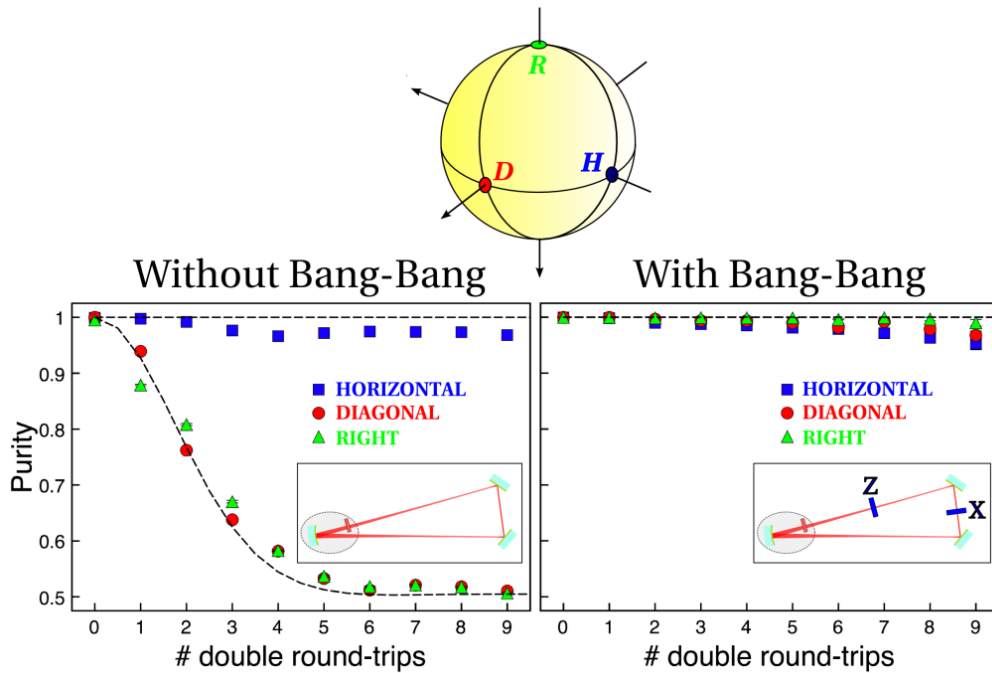


FIG. 3: **Purity versus the number of bang-bang cycles** for three different input polarization states. Horizontal polarization H is well preserved even without BB. On the contrary, if BB is not applied, the states D and R quickly decay in a Gaussian way (see Methods) to the fully mixed state, corresponding to a purity equal to $1/2$. On the contrary, when BB is applied the purity remains very close to one for the whole duration of the photon storage in the cavity.

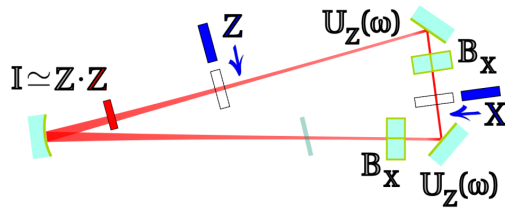


FIG. 4: **Schematics of the modified apparatus for arbitrary polarization decoherence.** A Soleil-Babinet is placed in front of each plane mirror at 45° . The Soleil-Babinet together with a plane mirror form the decohering element described by the operator $\mathbb{N}(\omega) = \mathbb{M}_Z[\phi(\omega)] \mathbb{B}_X[\theta]$. The waveplate denoted with \mathbf{Z} is placed in front of the spherical mirror in order to compensate its operation. The BB control operations \mathbb{X} and \mathbb{Z} of the Pauli-group decoupling are realized respectively by: i) adding to the phase of the Soleil-Babinet in the short arm of the cavity a delay equal to $\lambda/2$, so that its action on the polarization state is described by the Pauli matrix \mathbb{X} ; ii) by adding a second $\lambda/2$ wave-plate in the upper long arm.

For example, in a single mode fiber, birefringence and the orientation of the local principal axes of polarization are constant over a small fraction of the fiber beat length [26]. Few round-trips of our ring-cavity well mimic such a small portion, and our results show that, by applying a Pauli-group decoupling cycle within such a portion, one would preserve the polarization state. The decoherence strength and orientation will be different in the subsequent portions of the channel, but since BB inhibits decoherence for every θ , especially for few round-trips, one expects that by periodically repeating the Pauli-group decoupling cycle along the whole channel the polarization qubit can be preserved for distances much longer than currently achieved [25].

As a final remark we note that the BB polarization control demonstrated here is fundamentally different from the technique of Passive Compensation (PC), often used in quantum communication schemes [27]. PC exploits the retracing property of a beam traveling back and forth between two mirrors to revert on every “backward path” the dephasing introduced by dispersive elements during each “forward path”. Therefore, PC only works for *two-way* channels, as exemplified by the Faraday-PC [28]. Also the demonstration in [29] works only for a linear cavity and requires PC as an essential tool. On the contrary, in the present ring cavity, the photon always travels in the forward direction, thus proving the BB effectiveness in the more demanding task of flying qubit coherence-maintenance on a

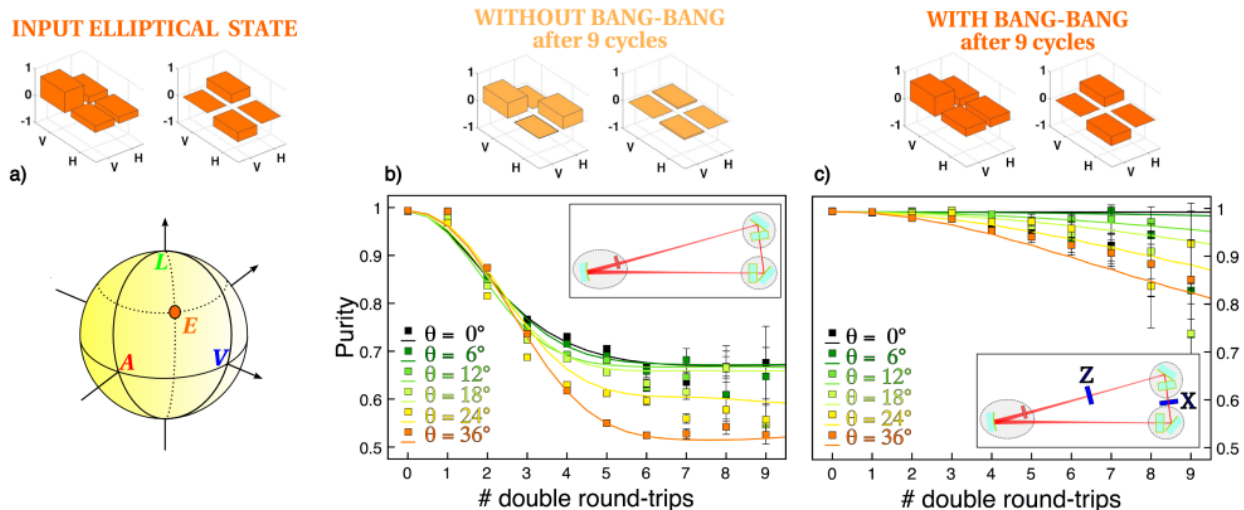


FIG. 5: **Evolution of an elliptical input state under generic decoherence.** a) Real and imaginary part of the density matrix, and position on the Bloch sphere of the input elliptical polarization state E . b) Real and imaginary part of the density matrix *without* BB after 9 double round-trips for $\theta = 24^\circ$, and purity of the output state vs the number of round-trips for different orientation θ of the Soleil-Babinetes. c) Real and imaginary part of the density matrix *with* BB after 9 double round-trips for $\theta = 24^\circ$, and purity of the output state vs the number of round-trips for different orientation θ of the Soleil-Babinetes. For each orientation of the decoherence-axis, the output purity with BB is significantly higher than the corresponding value without BB. However, purity preservation is not as good as in Figure 3 and worsens for increasing θ . In fact, when decoherence acts along an unknown basis, Pauli-group decouples a qubit from the environment at first order in the variance σ_ϕ^2 of the relative phase difference ϕ (see Methods).

one-way channel.

Acknowledgements

This work has been partly supported by the European Commission through FP6 under the Integrated Project ‘Qubit Applications’ QAP funded by the IST, Contract No. 015848. We thank L. Viola for many illuminating discussions and suggestions and G. Lo Bianco for the assistance with acquisition electronics.

-
- [1] Zurek, W. H. Decoherence, einselection, and the quantum origins of the classical. *Review Modern Physics* **75**, 715–775 (2003).
 - [2] Viola, L. & Lloyd, S. Dynamical suppression of decoherence in two-state quantum systems. *Physical Review A* **58**, 2733 (1998).
 - [3] Viola, L., Knill, E. & Lloyd, S. Dynamical decoupling of open quantum systems. *Physical Review Letters* **82**, 2417 (1999).
 - [4] Vitali, D. & Tombesi, P. Using parity kicks for decoherence control. *Physical Review A* **59**, 4178–4186 (1999).
 - [5] Zanardi, P. Symmetrizing evolutions. *Physics Letters A* **258**, 77–82 (1999).
 - [6] Kofman, A. G. & Kurizki, G. Unified theory of dynamically suppressed qubit decoherence in thermal baths. *Physical Review Letters* **93**, 130406 (2004).
 - [7] Facchi, P. *et al.* Control of decoherence: Analysis and comparison of three different strategies. *Physical Review A* **71**, 022302 (2005).
 - [8] Viola, L. *et al.* Experimental Realization of Noiseless Subsystems for Quantum Information Processing. *Science* **293**, 2059–2063 (2001).
 - [9] Morton, J. J. L. *et al.* Bang–bang control of fullerene qubits using ultrafast phase gates. *Nature Physics* **2**, 40–43 (2006).
 - [10] Fraval, E., Sellars, M. J. & Longdell, J. J. Dynamic decoherence control of a solid-state nuclear-quadrupole qubit. *Physical Review Letters* **95**, 030506 (2005).
 - [11] Ernst, R., Bodenhausen, G. & Wokaun, A. *Principles of Nuclear Magnetic Resonance in One and Two Dimensions* (Clarendon Press, Oxford, 1987).
 - [12] Shor, P. W. Scheme for reducing decoherence in quantum computer memory. *Physical Review A* **52**, R2493–R2496 (1995).
 - [13] Steane, A. M. Efficient fault-tolerant quantum computing. *Nature* **399**, 124–126 (1999).
 - [14] Chiaverini, J. *et al.* Realization of quantum error correction. *Nature* **432**, 602–605 (2004).
 - [15] Boulant, N., Viola, L., Fortunato, E. M. & Cory, D. G. Experimental implementation of a concatenated quantum error-

- correcting code. *Physical Review Letters* **94**, 130501 (2005).
- [16] Zanardi, P. & Rasetti, M. Noiseless quantum codes. *Physical Review Letters* **79**, 3306–3309 (1997).
- [17] Kielpinski, D. *et al.* A Decoherence-Free Quantum Memory Using Trapped Ions. *Science* **291**, 1013–1015 (2001).
- [18] Prevedel, R. *et al.* Experimental demonstration of decoherence-free one-way information transfer. *Physical Review Letters* **99**, 250503 (2007).
- [19] Vitali, D., Tombesi, P. & Milburn, G. J. Controlling the decoherence of a "meter" via stroboscopic feedback. *Physical Review Letters* **79**, 2442–2445 (1997).
- [20] Agarwal, G. S., Scully, M. O. & Walther, H. Inhibition of decoherence due to decay in a continuum. *Physical Review Letters* **86**, 4271–4274 (2001).
- [21] Search, C. & Berman, P. R. Suppression of magnetic state decoherence using ultrafast optical pulses. *Physical Review Letters* **85**, 2272–2275 (2000).
- [22] Vitali, D. & Tombesi, P. Heating and decoherence suppression using decoupling techniques. *Physical Review A* **65**, 012305 (2001).
- [23] Wu, L.-A. & Lidar, D. A. Overcoming quantum noise in optical fibers. *Physical Review A* **70**, 062310 (2004).
- [24] James, D. F. V., Kwiat, P. G., Munro, W. J. & White, A. G. Measurement of qubits. *Physical Review A* **64**, 052312 (2001).
- [25] Massar, S. & Popescu, S. Reducing polarization mode dispersion with controlled polarization rotations. *New Journal of Physics* **9**, 158 (2007).
- [26] A. Galtarossa, M. S., L. Palmieri & Tambosso, T. Measurements of beat length and perturbation length in long single-mode fibers. *Optics Letters* **25**, 384–386 (2000).
- [27] Gisin, N. & Thew, R. Quantum communication. *Nature Photonics* **1**, 165–171 (2007).
- [28] Martinelli, M. A universal compensator for polarization changes induced by birefringence on a retracing beam. *Optics Communications* **72**, 341–344 (1989).
- [29] Berglund, A. Quantum coherence and control in one- and two-photon optical systems. *quant-ph/0010001* (2000).
- [30] Azzam, R. M. A. & Bashara, N. M. *Ellipsometry and Polarized Light* (North-Holland, Amsterdam, 1977).

METHODS

Propagator. In order to fix a unique reference frame between theory and experiment we choose $|V\rangle$ ($|H\rangle$) to be the linear polarization state orthogonal (parallel) to the plane of the cavity, and denote with $\mathbb{Z} = |H\rangle\langle H| - |V\rangle\langle V|$ the Pauli matrix with eigenstates $|V\rangle$ and $|H\rangle$. The action of a cavity mirror on the polarization state is represented by the unitary operator $\mathbb{U}_{\mathbb{Z}}(\omega) = \exp[-i\phi_H(\omega)]|H\rangle\langle H| + \exp[-i(\phi_V(\omega) + \pi)]|V\rangle\langle V|$ [30] which, apart from an unessential global phase factor, can be rewritten as $\mathbb{U}_{\mathbb{Z}}(\omega) = \mathbb{Z}\mathbb{M}_{\mathbb{Z}}[\phi(\omega)]$, with $\phi(\omega) = \phi_H(\omega) - \phi_V(\omega)$ the relative phase due to the polarization-reflectivity difference and where $\mathbb{M}_{\mathbb{Z}}[\phi(\omega)] = \exp[-i\phi(\omega)\mathbb{Z}/2]$ represents the coupling between modes introduced by the mirror. The action of the S-B on the polarization state is described by $\mathbb{B}_{\mathbb{X}}[\theta] = \exp[-i\theta\mathbb{X}/2]$, with the Pauli matrix $\mathbb{X} = |H\rangle\langle V| + |V\rangle\langle H|$. We analyze in more detail the main sequence of operators entailed by the scheme. The combination of the S-B with a plane mirror realizes a *generalized noise operator* given by

$$\mathbb{U}_{\mathbb{N}}(\omega) = \mathbb{U}_{\mathbb{Z}}[\phi(\omega)]\mathbb{B}_{\mathbb{X}}[\theta] = \mathbb{Z}\mathbb{N}[\phi(\omega), \theta]. \quad (2)$$

which in the limit $\theta \rightarrow 0$ reduces to $\mathbb{Z}\mathbb{M}_{\mathbb{Z}}[\phi(\omega)]$. The main BB-decoupling cycle is obtained starting from the output mirror and listing down all the operators encountered by the photon in the cavity before it meets the output mirror a second time: $\mathbb{Z}\mathbb{N}[\phi(\omega), \theta]\mathbb{X}\mathbb{N}[\phi(\omega), \theta']$. As this propagator realizes only half of the Pauli-group decoupling, the complete cycle is obtained after any even number ($2n$) of cavity round-trips

$$\mathbb{U}_n^{\text{BB}}(\omega) = \{\mathbb{Z}\mathbb{N}[\phi(\omega), \theta]\mathbb{X}\mathbb{N}[\phi(\omega), \theta']\mathbb{Z}\mathbb{N}[\phi(\omega), \theta]\mathbb{X}\mathbb{N}[\phi(\omega), \theta']\}^n \quad (3)$$

In the case when the S-B do not introduce any phase shift ($\theta = \theta' = 0$), the direction of the axis of the polarization state unaffected by decoherence is known (z in this case) and perfect decoherence suppression is obtained. In this particular case the \mathbb{Z} operation of the Pauli-group cycle is superfluous and decoupling is also realized by the simpler Carr-Purcell BB cycle [3] requiring only one operation along a direction orthogonal to the decoherence axis (\mathbb{X} in this case).

Output purity and fidelity. We adopt the Bloch-sphere representation and write the input polarization state as $\rho_{in} = |\pi\rangle_{in}\langle\pi| = [I + \vec{P}_{in} \cdot \vec{\sigma}]/2$, where \vec{P}_{in} is the Bloch vector of the (pure) input polarization state and $\vec{\sigma} = (\mathbb{X}, \mathbb{Y}, \mathbb{Z})$. The output polarization state is given by the frequency average of Eq. (1) and can be written as $\rho_{out} = [I + \vec{P}_{out} \cdot \vec{\sigma}]/2$. It can be mixed and therefore $|\vec{P}_{out}| \leq 1$. The integral over the frequency can be treated by assuming a Gaussian spectrum for the input pulse, given by $\mathcal{E}(\omega) = (\pi\sigma_\omega^2)^{-1/4} \exp[-(\omega - \omega_0)^2/2\sigma_\omega^2]$, where σ_ω represents the bandwidth of the radiation spectrum centered in ω_0 . The frequency dependence enters through the relative phase $\phi(\omega)$ due to the polarization-reflectivity difference at the plane mirrors. This dependence is well described by the linear relation $\phi(\omega) \simeq \phi_0 + \tau(\omega - \omega_0)$, where $\phi_0 = \phi(\omega_0)$, so that the integral can be transformed into an average over a Gaussian measure with standard deviation $\sigma_\phi = \tau\sigma_\omega$,

$$\hat{\rho}_{out} = \int d\phi \frac{\exp\left[-\frac{(\phi - \phi_0)^2}{\sigma_\phi^2}\right]}{\sqrt{\pi\sigma_\phi^2}} [\mathbb{U}(\phi)]^n \rho_{in} [\mathbb{U}^\dagger(\phi)]^n, \quad (4)$$

where $\mathbb{U}(\phi)$ is the unitary operator describing the polarization transformation after one cavity round-trip (for a given frequency component). $\mathbb{U}(\phi)$ can always be expressed as $\mathbb{U}(\phi) = \exp[-i\alpha(\phi)\vec{s}(\phi) \cdot \vec{\sigma}]$, i.e., a rotation in the Bloch-sphere of an angle 2α around the axis individuated by the unit-norm vector \vec{s} . The BB and the no-BB case differ only in the expressions of $\alpha(\phi)$ and $\vec{s}(\phi)$. The Gaussian average of Eq. (4) can be explicitly performed if the pulse is not too broad, $\sigma_\phi \ll \pi$, which is well verified in our experiment. In this case, α and \vec{s} do not vary appreciably over the range of relevant phase shifts ϕ and one can approximate $\vec{s}(\phi)$ with its value at the pulse center $\vec{s}(\phi_0)$, while $\alpha(\phi)$ can be approximated by its second-order expansion around ϕ_0 , $\alpha(\phi) \simeq \alpha_0 + \dot{\alpha}_0(\phi - \phi_0) + \ddot{\alpha}_0(\phi - \phi_0)^2/2$.

From the output density matrix one derives the expression of the purity as a function of n (see Supplementary Informations). In the limit $n \rightarrow \infty$ purity tends to $\{1 + [\vec{P}_{in} \cdot \vec{s}(\phi_0)]^2\}/2$, which corresponds to the existence of a ‘‘pointer’’ basis unaffected by decoherence [1] (analogous to the principal states of polarization in fibers), formed by the two states with Bloch vector equal to $\pm\vec{s}(\phi_0)$. However, the interesting regime of our experiment is the one for *small* number of cavity round-trips n , where our ring-cavity well mimics a portion of a fiber with constant dispersive properties. For small n one has

$$\text{Tr}\{\hat{\rho}_{out}^2\} \simeq 1 - n^2 \left[\dot{\alpha}_0^2 \sigma_\phi^2 + \ddot{\alpha}_0^2 \frac{\sigma_\phi^4}{4} \right] \{1 - [\vec{P}_{in} \cdot \vec{s}(\phi_0)]^2\}, \quad (5)$$

showing that decoherence is best suppressed when $\dot{\alpha}_0$ and $\ddot{\alpha}_0$ are as small as possible. This condition means weak effective dispersion, because α depends upon ϕ just due to dispersion. BB Pauli-group decoupling suppresses decoherence by yielding $\dot{\alpha}_0 = 0$ so that for small n decoherence acts only at *fourth-order* in the small parameter σ_ϕ . This

fact can be seen from the expression of $\alpha(\phi)$ for the BB and no-BB case. Without BB, $\alpha(\phi)$ is given by the implicit expression $\cos \alpha = \cos \phi \cos^2 \theta/2 + \sin^2 \theta/2$, while with BB the implicit relation for α becomes $\cos \alpha = -(\sin \phi \sin \theta)/2$, implying that BB decoupling is realized for a generic θ when $\phi_0 \simeq \pi/2$.

When $\theta = 0$, which corresponds to the first experiment without the S-B, the situation considerably simplifies because $\alpha^{BB} = \pi/2$ does not depend upon ϕ so that BB Pauli-group decoupling suppresses decoherence at all orders in σ_ϕ , for every input polarization. Without BB it is $\vec{s}(\phi_0) = \hat{z}$, so that H and V are unaffected by decoherence, and $\alpha^{noBB} = \phi \Rightarrow \hat{\alpha}_0^{noBB} = 1$. As a consequence, the purity for input D and R polarizations has a Gaussian decay $[1 + \exp(-2n^2\sigma_\phi^2)]/2$, as confirmed by Figure 3. This result can be used for a best fit on the experimental data of Fig. 3, which gives $\sigma_\phi^{est}/\pi = (2.67 \pm 0.01) \times 10^{-2}$ rad. This value is consistent with the relation $\sigma_\phi = 2\pi c\tau\Delta\lambda/\lambda_0^2$ and with the measured value of the pulse spread $\Delta\lambda \simeq 15$ nm. Moreover, the estimated value for σ_ϕ is also consistent with our starting assumption $\sigma_\phi \ll \pi$.

Cavity and acquisition electronics. The triangular cavity, shown in Figure 1a, is formed by a spherical mirror with radius of curvature 1 m and reflectivity 98% and two flat mirrors with reflectivity 99%. The aperture angle of the cavity at the spherical mirror is $\sim 8^\circ$. The long arms of the cavity are ~ 0.94 m and the short arm is ~ 0.13 m determining a total cavity length of ~ 2.01 m, compatible with the measured time of a single round-trip of 6.80 ns. A signal from a function generator triggers a ~ 100 ps pulsed diode laser and starts the acquisition on the TAC. The output signal of a single-photon detector with quantum efficiency $\sim 70\%$, is sent to the stop-input of the TAC and then to the MCA for data recording. The MCA has a resolution of 8192 channels. The acquisition electronics has a time-resolution of ~ 102 ps.

Data analysis. The density matrices are evaluated by maximum-likelihood estimation from the histogram obtained with the TAC/MCA system for different settings of the waveplates in the tomography apparatus. Ten time-bins around each peak of the histograms, corresponding to an integration time windows of ~ 1 ns, have been summed for evaluating the detector counts for the corresponding round-trip, C_p^j , with j the round trip index and p denoting the measured polarization.